AGU PUBLICATIONS
JGR
Journal of Geophysical Research: Oceans

RESEARCH ARTICLE
10.1002/2016JC011924

Key Points:
- Mixing of DO is controlled by interactions between wind-driven circulation and bathymetry
- Wind-driven Ekman dynamics advect low oxygen water onto shoals where mixing occurs
- Localized vertical mixing supplies DO to bottom waters that is advected up-Bay

Correspondence to:
M. E. Scully,
mscully@whoi.edu

Citation:
Scully, M. E. (2016), Mixing of dissolved oxygen in Chesapeake Bay driven by the interaction between wind-driven circulation and estuarine bathymetry, *J. Geophys. Res. Oceans*, *121*, 5639–5654, doi:10.1002/2016JC011924.

Received 29 APR 2016
Accepted 8 JUL 2016
Accepted article online 13 JUL 2016
Published online 8 AUG 2016

Mixing of dissolved oxygen in Chesapeake Bay driven by the interaction between wind-driven circulation and estuarine bathymetry

Malcolm E. Scully[1]

[1]Applied Ocean Physics and Engineering, Woods Hole Oceanographic Institution, Woods Hole, Massachusetts, USA

Abstract Field observations collected in Chesapeake Bay demonstrate how wind-driven circulation interacts with estuarine bathymetry to control when and where the vertical mixing of dissolved oxygen occurs. In the across-Bay direction, the lateral Ekman response to along-Bay wind forcing contributes to the vertical mixing of dissolved oxygen in two ways. First, the lateral tilting of the pycnocline/oxycline, consistent with the thermal wind relationship, advects the region of high vertical gradient into the surface and bottom boundary layers where mixing can occur. Second, upwelling of low-oxygen water to the surface enhances the atmospheric influx. In the along-Bay direction, the abrupt change in bottom depth associated with Rappahannock Shoal results in surface convergence and downwelling, leading to localized vertical mixing. Water that is mixed on the shoal is entrained into the up-Bay residual bottom flow resulting in increases in bottom dissolved oxygen that propagate up the system. The increases in dissolved oxygen are often associated with increases in temperature and decreases in salinity, consistent with vertical mixing. However, the lagged arrival moving northward suggests that the propagation of this signal up the Bay is due to advection.

1. Introduction

Low dissolved oxygen (DO) is one of the most pressing and visible water quality problems facing Chesapeake Bay. Billions of dollars have been spent to reduce nutrient loading to the Bay with a fundamental goal of reducing the extent and severity of hypoxia [*Butt and Brown*, 2000]. Despite significant efforts to reduce nutrient loading, large volumes of the Bay continue to be impacted by hypoxia and anoxia and studies that directly relate nutrient loading to hypoxic volume often fail to explain the majority of the observed variability [*Hagy et al*., 2004; *Murphy et al*., 2011]. One fundamental problem in assessing efforts to improve water quality in Chesapeake Bay and other estuarine systems is a complete understanding of the physical processes that modulate DO [*Kemp et al*., 2009; *Scully*, 2010a].

Early studies demonstrated that hypoxic conditions develop when oxygen utilization rates exceed replenishment across the pycnocline by turbulent mixing [*Taft et al*., 1980; *Officer et al*., 1984]. The occurrence of hypoxic conditions during the summer months is thought to be the result of increased respiration rates fueled by primary production and decreased vertical mixing caused by the increase in vertical density stratification in response to elevated spring river discharge [*Seliger et al*., 1985]. Warmer water and weaker wind mixing also contribute to reduced oxygen levels during the summer months. These early studies provided a basic conceptual model for hypoxia that was one-dimensional in the vertical. *Malone et al*. [1986] suggested that the rotational response of the pycnocline to wind-driven forcing might provide an important mechanism for the lateral exchange of DO between the surface and subpycnocline waters, challenging the simple 1-D conceptual model. *Sanford et al*. [1990] also documented significant variability in near-bed oxygen concentrations at a variety of time scales that were attributed to the coupled vertical and lateral motions of the pycnocline.

The use of numerical circulation models to simulate oxygen dynamics has improved our understanding of the physical processes that modulate hypoxia and demonstrated that advection and mixing of DO in Chesapeake Bay has significant three-dimensional variability. *Scully* [2010b] used a highly simplified DO module in a realistic circulation model of Chesapeake Bay to demonstrate that the interaction between wind-driven

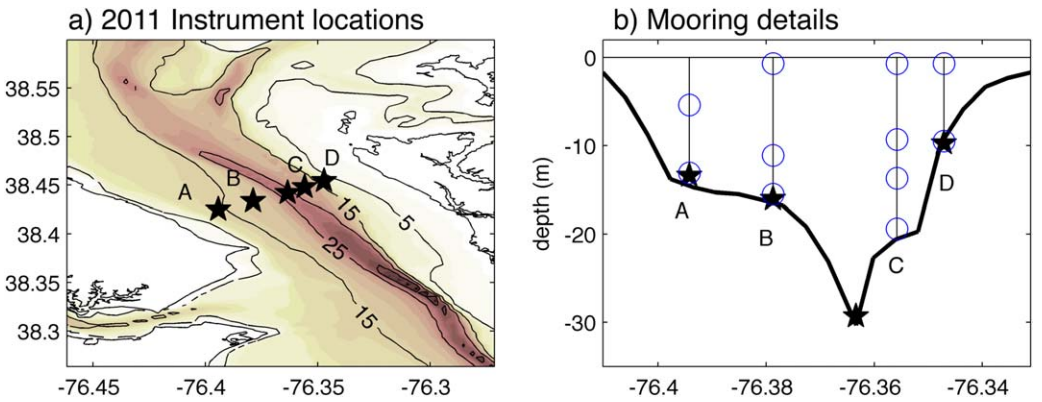

Figure 1. (a) Location of the instruments deployed in the 2011 field campaign in Chesapeake Bay. Stars denote instrument locations and bathymetry is shown in color. (b) Vertical location of instruments on moorings in the mid-Bay cross section. Blue circles denote CTDs with integrated dissolved oxygen sensors and black stars denote the locations of bottom mounted ADCPs. For 2011, moorings are named A, B, C, and D moving from west to east.

lateral circulation and enhanced vertical mixing over shoal regions is the dominant mechanism for providing oxygen to hypoxic subpycnocline waters. Using a similar approach, *Scully* [2013] demonstrated that the seasonal cycle of hypoxia in Chesapeake Bay was strongly controlled by physical processes, particularly the seasonal variations in wind speed and direction. In that study, the wind direction was shown to play an important role in controlling the along-Bay advective flux of DO. The results of *Li et al*. [2015] suggest that hypoxia was relatively insensitive to changes in river discharge because of the compensatory effect of decreased vertical mixing and increased longitudinal advection in response to increased river discharge.

To date, these dynamics have not been conclusively demonstrated using field data. This is largely because field observations with sufficient spatial and temporal resolution have not been made. In Chesapeake Bay, the primary source of oxygen data for model evaluation is the Chesapeake Bay Program (CBP) water quality data. The CBP water quality cruises began in 1984 and collect a comprehensive suite of physical and biogeochemical data throughout the Bay and its tributaries. The cruises occur every month, except during the summer months, when two cruises per month are conducted. While this database is a valuable resource, the data have relatively coarse temporal resolution with each "cruise" consisting of sampling conducted from multiple research vessels over the course of several days. As a result, the data often are not synoptic in time and cannot resolve processes with frequencies higher than several weeks. Further, cruises are often delayed by bad weather when large changes in DO may occur. Thus, CBP data are sufficient for providing a bulk characterization of the seasonal and interannual variations of hypoxia in the Bay, but they are not adequate for resolving the response to episodic events. Similarly, few if any, numerical models have been validated against DO data with high sampling frequency so their ability to accurately simulate these events remains untested.

This paper presents detailed field observations of DO collected with high spatial and temporal resolution. The data were collected during two intensive field experiments. The first experiment spanned the summer of 2011 and focused on the spatial and temporal variability of DO at a mid-Bay estuarine cross section. The second campaign spanned the summer of 2013 and focused on the spatial and temporal variability along the main axis of the Bay. Section 2 provides the details of the instrumentation and sampling used during the two intensive field campaigns. The results are presented in section 3, examining the lateral and longitudinal response to wind forcing separately. The results are discussed and conclusions are presented in section 4.

2. Methods

During the summer of 2011, four moorings and four bottom landers were deployed across a mid-Bay transect roughly 12 km north of the mouth of the Patuxent River, MD (Figure 1a). Moving from west to east, the mooring locations are referred to as mooring A, B, C, and D. At each mooring, salinity, temperature, and DO were measured using Seabird Electronics SBE37-SMP-IDO microcat CTDs at multiple depths (see Figure 1b). A bottom frame with upward looking acoustic Doppler current profiler (ADCP) was deployed immediately adjacent to moorings A, B, and D to measure full water column profiles of current velocity. An additional

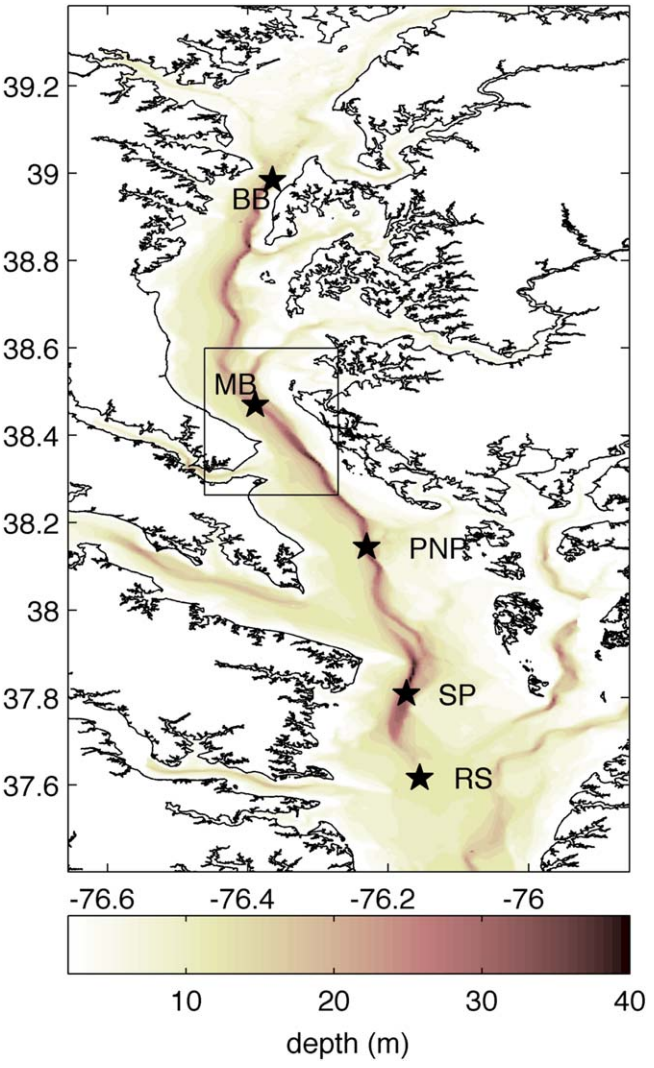

Figure 2. Location of the instruments deployed in the 2013 field campaign in Chesapeake Bay, denoted by black stars, superimposed on the estuarine bathymetry. The instrument locations are named for local geographic locations and moving from north to south are BB (Bay Bridge), MB (Mid Bay), PNP (Point No Point), SP (Smith Point), and RS (Rappahannock Shoal). At all locations a bottom mounted CTD with integrated dissolved sensor was deployed. All locations except RS had an upward looking ADCP. A bottom-mounted ADV measured currents at RS. The black box indicates the region shown in Figure 1a.

bottom mounted ADCP was deployed in the deepest part of the channel, where shipping traffic prevents the safe deployment of a mooring. Each CTD sampled every 3 min and the ADCPs sampled every 6 min. The instrumentation was deployed from 20 May to 12 July 2011 and from 23 July to 27 September 2011. Between the two deployments in 2011, the instruments were serviced. The surface CTD at mooring A malfunctioned, providing no data from this location. The surface CTDs at moorings B and C and the bottom CTD at mooring D were destroyed in late August during the passage of Hurricane Irene, limiting data from these locations to the first deployment (20 May to 12 July).

During the summer of 2013 five bottom landers were deployed along the main axis of the Bay (Figure 2). The locations are identified using local geographic names and moving from north to south are referred to as Bay Bridge (BB), Mid Bay (MB), Point No Point (PNP), Smith Point (SP), and Rappahannock Shoal (RS). All of the bottom landers in 2013 had Seabird Electronics SBE37-SMP-IDO microcat CTDs measuring salinity, temperature, and DO at 6 min intervals. All of the bottom landers except (RS) had an upward looking ADCP. The bottom lander at RS had an acoustic Doppler velocimeter (ADV), which recorded near bottom velocity in 5 min bursts every hour. All of the ADCPs recorded velocity profiles every 6 min.

In 2013 the bottom landers were deployed on 18 April and recovered on 22 July 2013. Only the bottom landers in the deep channel north of RS (e.g., BB, MB, PNP, and SP) were redeployed after servicing. BB and SP were redeployed on 26 July and MB and PNP were redeployed on 22 August 2013. The four bottom landers were recovered in late October or early November 2013. The CTD at MB failed during the second deployment of 2013, but an additional bottom mounted CTD with DO sensor was deployed 750 m to the east of MB, as part of another project. The depth at this location was 23 m and this sensor is used in place of MB for the period from 21 August to 30 October 2013.

In addition to the in situ instrumentation that was deployed, ship-based surveys were conducted in both 2011 and 2013. In 2011, across-channel CTD transects were collected using a small boat and CTD equipped with a fast response Rinko optical oxygen sensor. The Rinko optode has a reported response time of 1 s and sampled at 6 Hz. Lateral transects were conducted in the vicinity of the mooring array where vertical profiles of salinity, temperature, and DO were sampled at 10 evenly spaced stations. In 2013, several along-Bay surveys were conducted from the R/V Hugh Sharp using a vertically undulating Scanfish. The Scanfish was

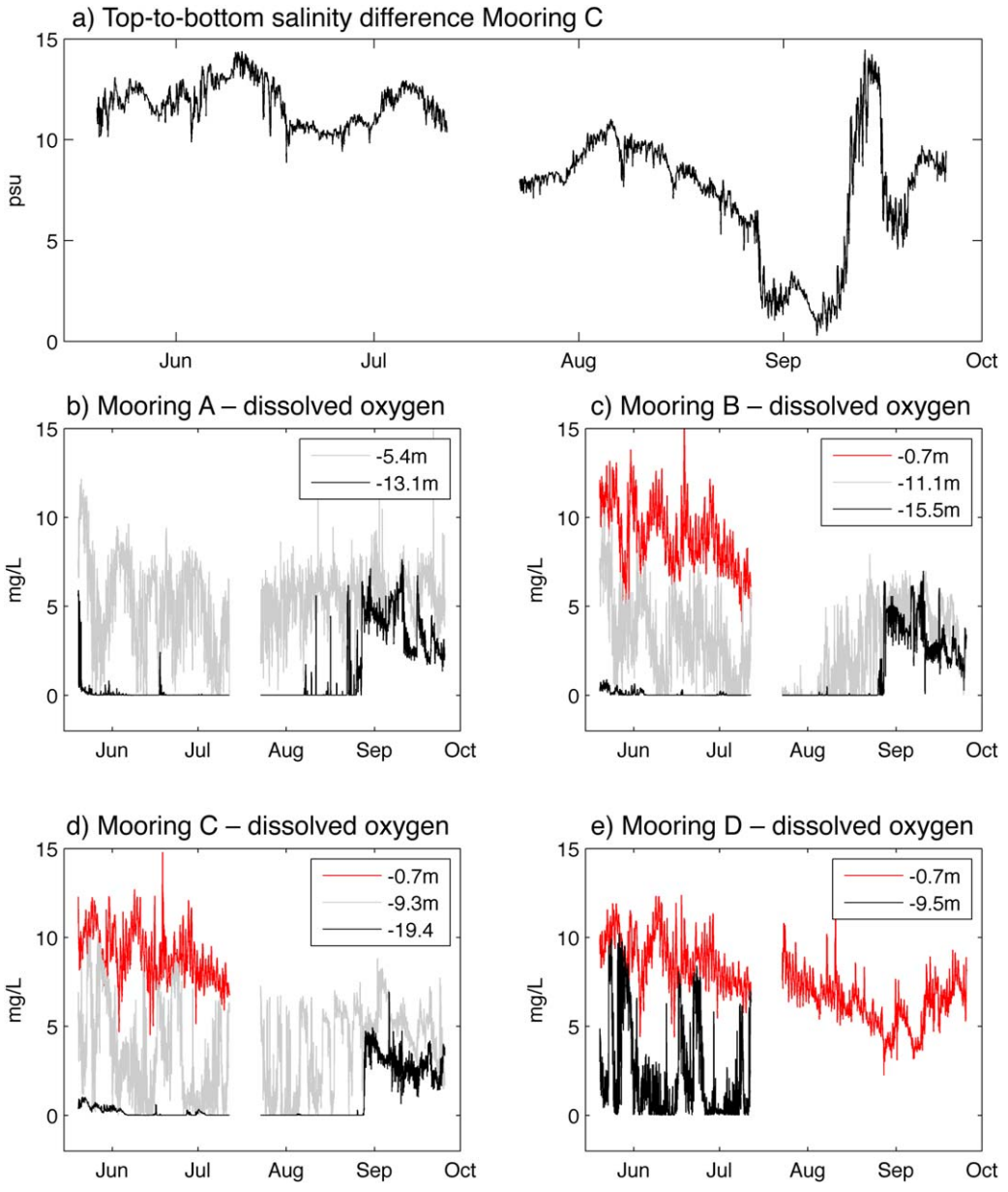

Figure 3. Mooring data from 2011 including: (a) time series of top-to-bottom salinity difference measured at mooring C; bottom dissolved oxygen concentration measured at (b) mooring A, (c) mooring B, (d) mooring C, and (e) mooring D. The mean depth from the surface for each sensor is indicated in the figure legend. The surface CTD at mooring C was destroyed in Hurricane Irene so the surface salinity from mooring D and bottom salinity from mooring C are used to calculate the top-to-bottom difference for 23 July to 27 September 2011.

equipment with a Seabird CTD and DO probe (SBE-43). The surveys generally began in the vicinity of the BB and continued beyond SP onto Rappahannock Shoal, following the main axis of the deep channel. The average vessel speed over ground was roughly 3 m/s and the Scanfish completed a full profile (up and down) approximately every 30 s providing ~0.2 m vertical resolution and ~100 m horizontal resolution. In both 2011 and 2013, only data from the down-casts were used.

3. Results

3.1. 2011 Field Season (Lateral Response)

The focus of the 2011 field season was on the DO variability in the across-channel direction. When the instruments were deployed in mid-May, there was strong vertical salinity stratification and the bottom

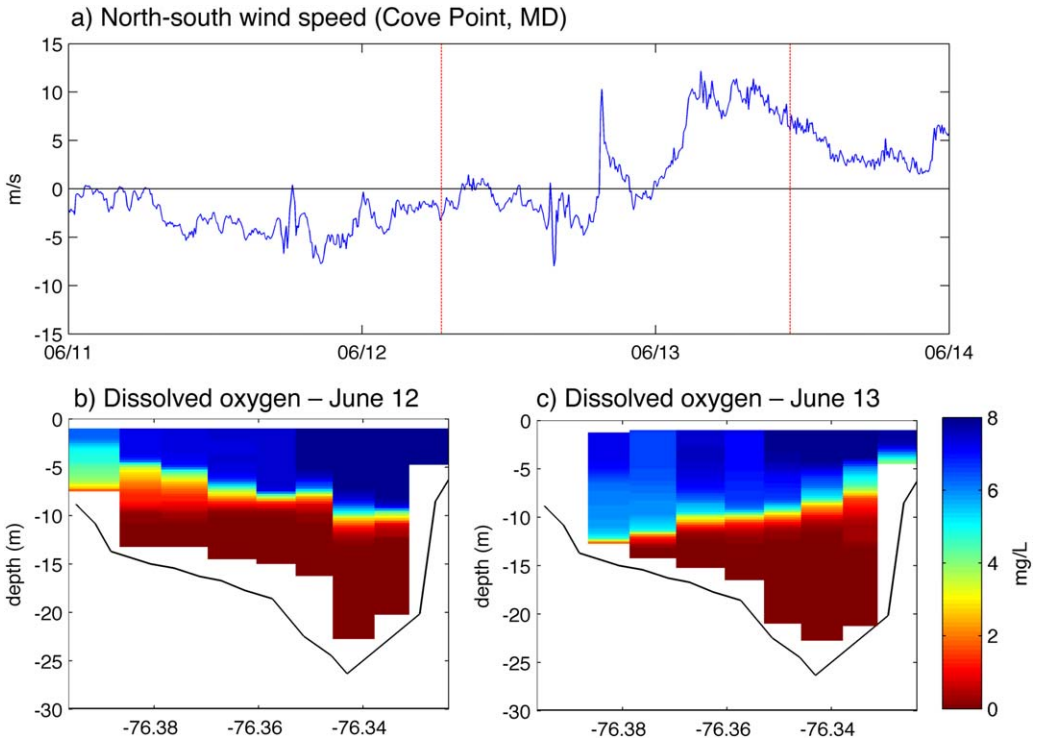

Figure 4. (a) North-south wind speed measured at Cove Point LNG Pier (NDBC station COVM2) encompassing period when ship-based lateral transects of dissolved oxygen were conducted. Vertical red lines indicate time of lateral transects; (b) lateral distribution of dissolved oxygen on 12 June following a period of winds from the south; (c) lateral distribution of dissolved oxygen on 13 June following a period of winds from north. The lateral transects were conducted immediately to the north of the moorings in 2011 shown in Figure 1.

oxygen had already dropped below 2 mg/L at all locations except mooring D (Figure 3). By early June, bottom DO at moorings A, B, and C was essentially zero and anoxic conditions were maintained almost continuously until late August when Hurricane Irene passed over the region. After the passage of Hurricane Irene, bottom DO concentration stayed above 2 mg/L at most locations until the instruments were recovered in late September. The vertical salinity stratification was reduced, but not eliminated, during the hurricane.

Unlike the other bottom locations, the bottom DO at mooring D was highly variable during the first deployment of 2011 (Figure 3d). At this location, bottom DO range from anoxic conditions to supersaturated, sometimes within hours (e.g., 26–27 May). The variability occurs at both tidal and synoptic time scales. At tidal time scales, DO increases are associated with decreases in salinity and generally occur during the flood tide. The opposite pattern is observed during ebb tides consistent with bottom Ekman dynamics. At synoptic time scales, high bottom DO concentration at mooring D occurs during wind events from the south and low DO concentration during wind from the north. The opposite pattern is observed at the mid water column DO sensor on mooring A. The lateral response of DO to along-Bay winds is consistent with wind-driven Ekman dynamics. Down-Bay winds (from the north) induce surface transport and downwelling to the west, and bottom transport and upwelling to the east. Up-Bay winds (from the south) drive the opposite pattern with downwelling along the eastern shore.

The impact of Ekman dynamics on the DO field is clearly seen from ship-based lateral surveys that were conducted in early June (Figure 4). The survey conducted on 12 June occurred after a period of moderate winds from the south. The interface between the upper oxygenated layer and the bottom anoxic water slopes upward toward the west. Following the survey on the 12 June there were relatively energetic winds from the north. The first survey after this down-Bay wind event shows that the interface slope has reversed, sloping upward toward the east. During the 12 June survey, the oxygen interface almost intersects the surface at the western shore and the width of the interface is much thicker at the western-most station than at the other locations. The following day, the interface is much lower in the water column intersecting the bed in roughly 15 m of water. While there are small lateral oscillations associated with tidal Ekman dynamics,

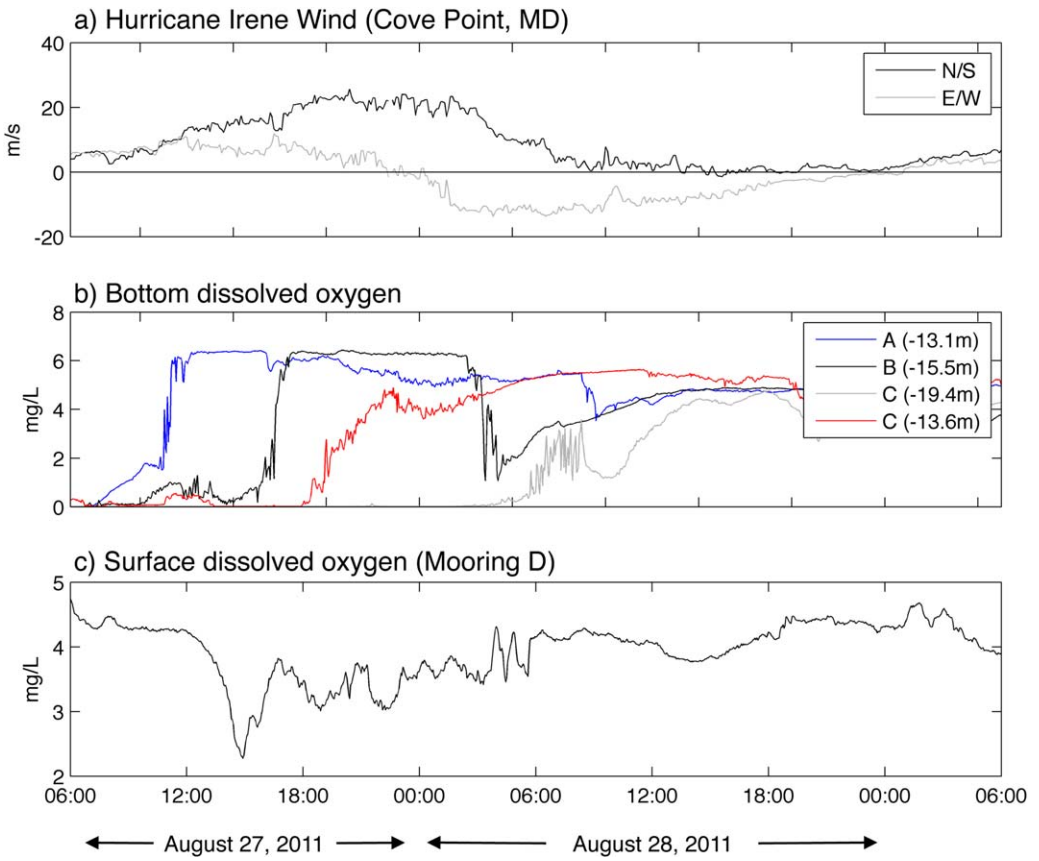

Figure 5. (a) Wind speed measured at Cove Point LNG Pier (NDBC station COVM2) during the passage of Hurricane Irene. Black line is the north-south component and gray line is east-west component of wind. Positive values are winds from north and from east; (b) corresponding time-series of bottom dissolved oxygen demonstrating how the rapid ventilation of bottom water proceeds from west to east arriving first at mooring A (blue line), followed by mooring B (black line), and mooring C (gray line). The increase in oxygen arrives at the sensor 13.6 m below the surface at mooring C (red line) after the bottom sensor at mooring D ($z \sim -15.5$ m) inconsistent with purely vertical mixing; (c) time series of surface dissolved oxygen at mooring D. Values fall to below 3 mg/L as tropical storm force winds develop.

the oscillations of the pycnocline are dominated by the response to along-Bay wind forcing (e.g., Figure 3). These large wind-driven vertical excursions bring the interface into the surface and bottom boundary layers, where tidal and wind mixing can more effectively mix oxygenated and hypoxic waters. The advection of low DO water to the surface also can enhance the air-sea flux as discussed below.

The passage of Hurricane Irene provides a dramatic illustration of the importance of the wind-driven lateral response to oxygen dynamics. Hurricane Irene moved up the east coast of the United States in late August, passing just off-shore of the mouth of Chesapeake Bay late on 27 August 2011. Sustained winds at the Cove Point LNG Pier (NDBC Buoy COVM2) exceeded 25 m/s during the peak of the storm and winds were almost exclusively from the north over Chesapeake Bay (Figure 5a). Winds diminished quickly as the storm moved up the coast. The moored CTD-DO data clearly show the rotational response to this strong down-Bay wind forcing. Bottom oxygen levels increase dramatically first at mooring A around 10:30 on 27 August (Figure 5b). Roughly 4 h later, the bottom DO increases rapidly at mooring B. Oxygen levels are not observed to increase at the bottom sensor at mooring C until roughly 19 h after the initial increase at mooring A, when winds are diminishing. DO concentration at $z \sim -13.6$ m at mooring C increases well after those at the bottom of mooring B, even though the bottom sensor at mooring B is farther from the surface.

At approximately the same time that the bottom DO is increasing rapidly at mooring B, the surface DO a mooring D is decreasing (Figure 5c). Despite the fact that the winds are in excess of 18 m/s, surface values of DO at mooring D drop below 2.5 mg/L. This drop in DO is consistent with the Ekman response to the strong down-Bay winds. Surface Ekman-driven downwelling along the western shore brings oxygenated waters to depth. This signal progresses from west to east as the winds intensify. At the same time, the

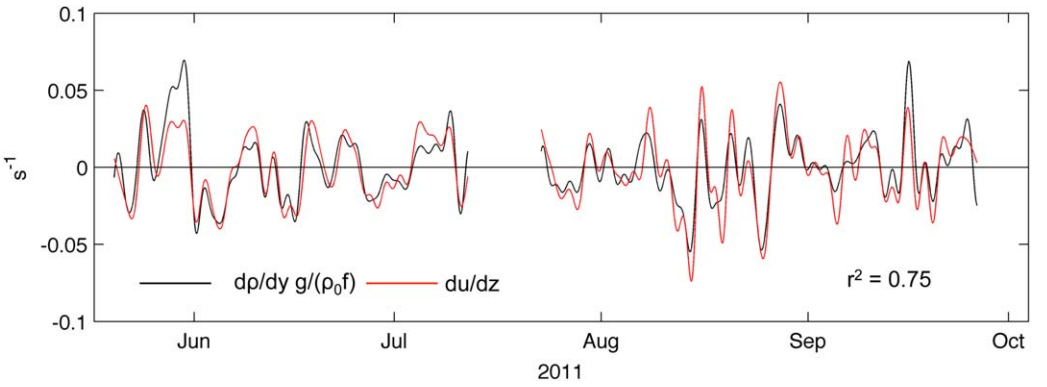

Figure 6. Subtidal thermal wind balance comparing the observed vertical shear (red line) to the appropriately scaled lateral density gradient (black line) in 2011. Vertical shear was calculated by differencing the along channel velocity measured 11 and 15 m from the surface by the ADCP deployed in the deepest part of the cross section. The lateral density gradient was calculated by differencing the bottom density at mooring A and the density measured −13.6 m from the surface at mooring C.

anoxic waters in the deep channel are displaced to the east, upwelling along the eastern shore. As these waters upwell, they are mixed by the strong surface winds. As a result, the surface waters at mooring D ($z \sim -0.7$ m) decrease to roughly 30% saturation under tropical storm force winds.

To more quantitatively evaluate the lateral dynamics, the moored data are used to estimate the thermal wind balance (e.g., $du/dz \sim g/(f\rho_0)\, d\rho/dy$). The lateral density gradient ($d\rho/dy$) is calculated by differencing the density measured by the bottom CTD on mooring A and the density measured by the CTD at roughly the same depth on mooring C (e.g., $z \sim -13.6$ m). The along-channel shear (du/dz) is calculated from the

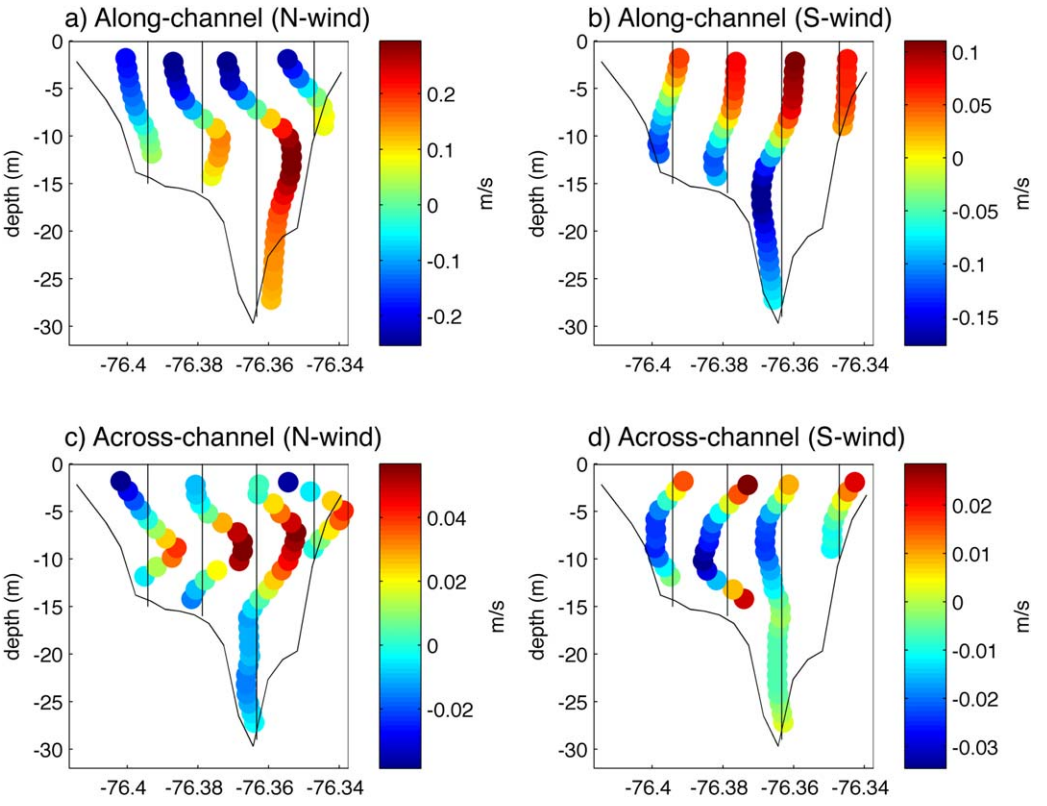

Figure 7. Residual along (a–b) and across (c–d) channel velocity structure measured by the four bottom mounted ADCPs in 2011. Data were averaged over all conditions when the N-S component of the wind measured at Cove Point LNG Pier was from the north and greater than 5 m/s (a and c) and from the south greater than 5 m/s (b, d). The strength of the velocity is denoted both quantitatively using the color scale (positive toward north and east) and qualitatively via the vertical structure.

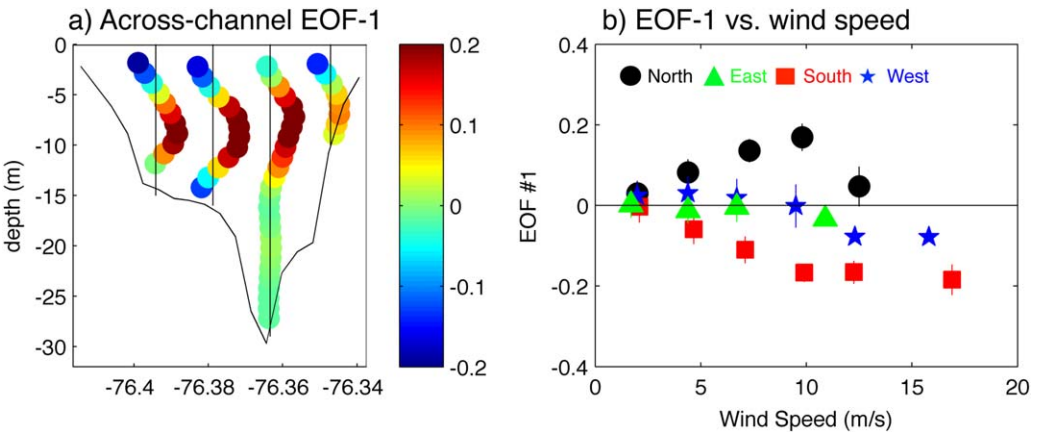

Figure 8. (a) Structure of the first-mode EOF for the across channel subtidal velocity in 2011, which is strongly correlated to the along-Bay wind speed ($r = 0.90$). (b) Principal component of the first-mode EOF bin-averaged as a function of wind speed for winds from the north (black circles), east (green triangles), south (red squares), west (blue stars). Vertical bars represent ± 1 standard deviation.

ADCP deployed in the deep channel using velocity bins that are separated by 4 m and centered on $z \sim -13$ m. The data are low-pass filtered with a 50 h cutoff to remove tidal variability, to focus on subtidal processes. Despite the relatively crude estimate of the lateral density gradient, there is strong agreement between the along-channel shear and lateral baroclinic forcing ($r^2 = 0.75$) (Figure 6). During periods of strong wind forcing, including the passage of Hurricane Irene, the observed along-channel shear exceeds the thermal wind value, suggesting that along-Bay wind stress enhances the vertical shear and that ageostrophic terms contribute to the lateral balance. Under strong winds (>7 m/s), the mid water column shear is positively correlated with the down-Bay winds ($r^2 = 0.73$) and correlation between the terms in the thermal wind balance increases ($r^2 = 0.83$). Even during the passage of Hurricane Irene, the top-to-bottom salinity difference never is reduced to zero and the water column remains stratified during the entire deployment (Figure 3a).

The along-channel residual velocity at this cross section is strongly modulated by the along-Bay wind stress. Winds from the north enhance the baroclinically driven two layer residual circulation, while winds from the south often reverse the mean two-layer circulation, with inflow near the surface and outflow at depth (Figures 7a and 7b). Consistent with the thermal wind balance, the zero isopleth slopes upward toward the east under moderate winds from the north and slopes upward to the west under moderate winds from the south. The first-mode empirical orthogonal function (EOF) for the subtidal along-channel velocity explains 60% of the variance and is strongly correlated to the north-south component of wind ($r = -0.83$) (data not shown).

The subtidal across-channel circulation is consistent with the Ekman response to the along-Bay wind stress. Winds from the north drive a near-surface lateral flow toward the west and winds from the south drive a near-surface lateral flow toward the east (Figures 7c and 7d). The surface Ekman layer extends down to a depth of approximately 4 m and is not completely resolved near the surface because of sidelobe interference of the ADCPs. The lateral circulation exhibits a clear two-layer response with flow in the opposite direction to the surface in the layer extending down to a depth of approximately 10 m. In the deep channel, lateral flows in the lower half of the water column are weak.

The strength and structure of the lateral circulation is quantified using EOF analysis of the subtidal lateral velocities (Figure 8a). The first-mode EOF explains 43% of the variance and is strongly correlated with the along-channel wind ($r = 0.90$). The time series of the first-mode principal component changes sign consistent with the Ekman response to along-Bay wind stress. For winds from the north and south, the strength of the lateral flow (as quantified by the first-mode EOF) increases monotonically up to a wind speed of 10 m/s (Figure 8b). At higher wind speeds, the strength of the lateral flow decreases slightly. The overall strength of the lateral flow when winds are from the west or east is weaker than for winds from the north or south, and winds from the west have the weakest response of the four wind directions considered.

The lateral response to wind forcing plays an important role in modulating the air-sea flux of DO. Up-Bay winds advect low-oxygen water onto the western shoal where water column mixing and surface exchange

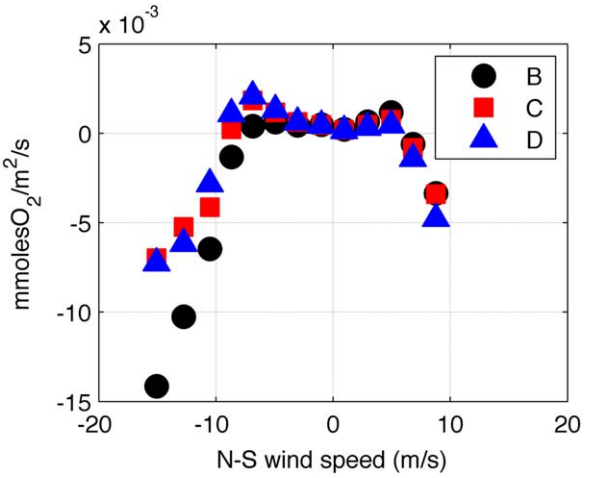

Figure 9. Surface flux of dissolved oxygen calculated using the wind speed dependent formulation of Wanninkhof (1992) and the dissolved oxygen concentration measured at z = −0.7 m on moorings B (black circles), C (red squares), and D (blue triangles) in 2011. Data have been bin-averaged as a function of the north-south wind velocity measured at Cove Point LNG Pier. Positive values indicate flux into the overlying atmosphere and negative values indicate flux into the water column.

can increase oxygen concentrations. Conversely, down-Bay winds enhance mixing and surface flux on the eastern shore. Estimates of surface oxygen flux are made using the wind speed-dependent gradient formulation proposed by *Wanninkhof* [1992]. Estimates of surface oxygen flux for each mooring with surface oxygen sensors are averaged as a function of the north-south wind speed (Figure 9). Under weak wind conditions the flux is generally positive (e.g., into atmosphere), consistent with super saturated near-surface DO concentrations. Strong winds from both the north and south result in significant oxygen fluxes into the Bay. However, there are asymmetries in this response as a function of wind direction. Under strong up-Bay winds, the surface flux at mooring B is roughly double that at moorings C and D. In this analysis the winds are assumed uniform over the study area so this enhanced inward flux at mooring B is solely driven by lower near-surface values of oxygen at this location. Although there are fewer strong wind events from the north during the summer deployment, the estimated surface fluxes at mooring D are generally

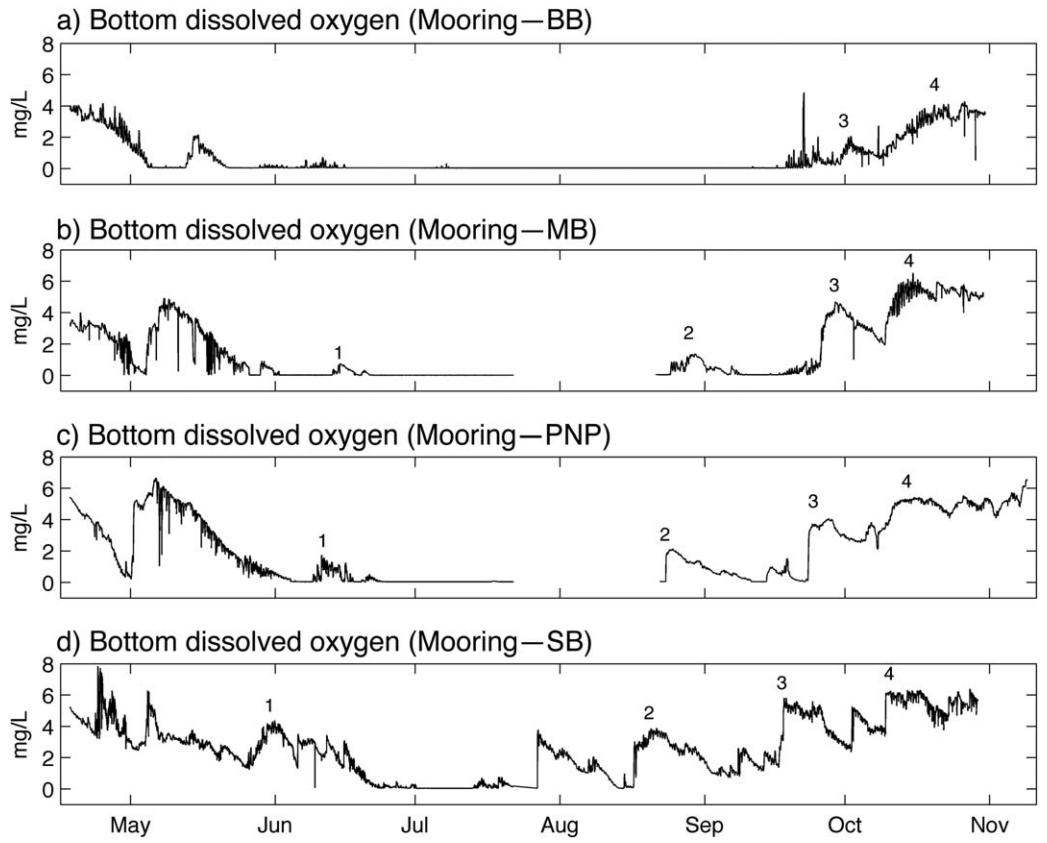

Figure 10. Time series of bottom dissolved oxygen measured during 2013 from moorings (a) BB, (b) MB, (c) PNP, and (d) SP. Numbers are used to identify "events" where increases in bottom dissolved oxygen are observed to propagate up the Bay.

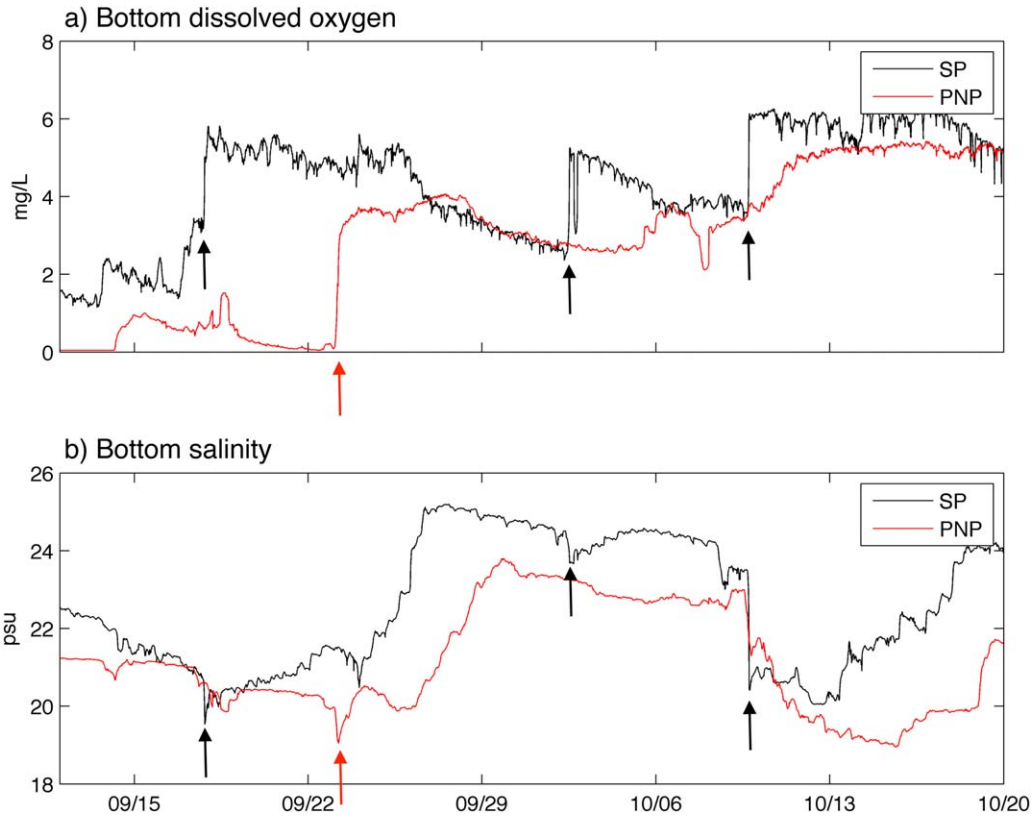

Figure 11. Detail of time series of (a) bottom dissolved oxygen and (b) salinity at moorings SP (black line) and PNP (red line) during Fall 2013. Arrows in Figures 11a and 11b are used to mark periods when dissolved oxygen increases rapidly, showing that these increases are often associated with drops in salinity.

larger (e.g., more negative) than at mooring B for the same wind speed because of the upwelling of low-oxygen waters along the eastern shore in response to winds from the north.

3.2. 2013 Field Season (Longitudinal Response)

The 2013 field experiment focused on the DO variability in the along-channel direction, with instruments spanning the deep central channel of the Bay. The instruments were deployed in mid-April when bottom oxygen levels were above 3 mg/L at all four of the deep locations (Figure 10). With the exception of at SP, values of bottom DO first drop below 2 mg/L in late April. At BB, DO is maintained below 2 mg/L for the period from 30 April to 11 October. The duration of persistent hypoxia decreases moving southward, with SP only experiencing continuous hypoxia for the period from 16 June to 26 July. There are other periods of low DO at SP, but episodic events that are characterized by rapid increases in DO occur roughly every 20–30 days, interrupting the continuous hypoxia at this location. The rapid increases in DO that are observed at SP are often observed at PNP and MB with a time lag of 5–6 and 8–10 days, respectively. The along estuary propagation of this signal corresponds to an advective velocity of roughly 0.08 m/s. The magnitude of the increases in DO typically is diminished as it propagates up the Bay.

Many of the rapid increases in DO that are observed at SP occur simultaneously with rapid decreases in salinity. For example, the rapid increases in DO at SP on 17 September, 2 October, and 9 October are all associated with decreases in salinity (Figure 11). Similar events are observed at PNP, and at both SP and PNP there is a negative correlation between the time rate of change of bottom salinity and DO. The coincident increases in oxygen and decreases in salinity are generally consistent with vertical mixing, but the phasing of these events along the system is not, and suggests that the observed changes in bottom DO are the result of along-channel advection. A crude estimate of the longitudinal advective flux (e.g., $u\Delta O_2/\Delta x$) at PNP can be calculated using a centered difference estimate of the bottom DO gradient between SP and MB and the observed along-channel near bed velocities (u) at PNP. The advective flux is compared to the

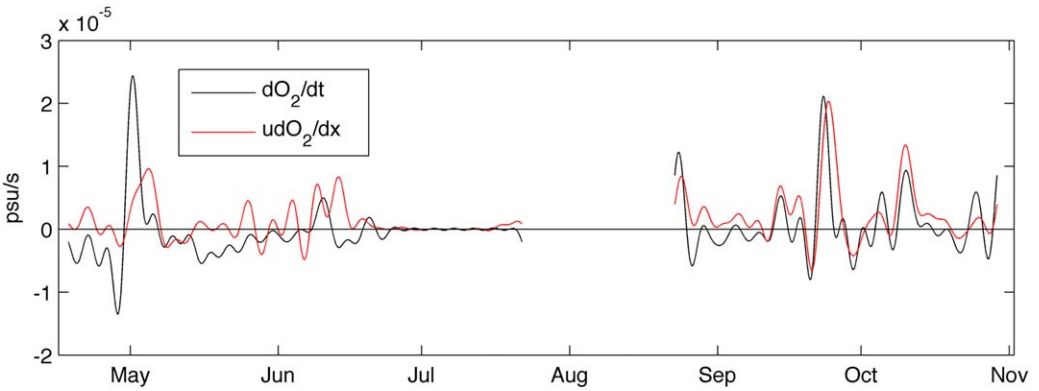

Figure 12. Comparison of the subtidal time rate of change of dissolved oxygen at mooring PNP (black line) with a simple estimate of the subtidal along-channel advection (red line) calculated from the bottom dissolved oxygen gradient observed between SP and MB and the observed near bed velocity at PNP. During the fall deployment the agreement is reasonable (r = 0.73) suggesting that the changes in dissolved oxygen observed at PNP are consistent with along-channel advection.

observed time rate of change of DO at PNP in Figure 12. During the first deployment, the agreement is relatively poor (r = 0.37); however, during the second deployment when the strong episodic increases in DO are frequent, the agreement is much stronger (r = 0.73). The timing and magnitude of the rapid increases in DO on 24 August, 23 September, and 10 October are all reasonably predicted by along-channel advection.

We hypothesize that mixing over Rappahannock Shoal creates the oxygenated waters that are advected up-Bay. A strong wind event from the North in late May (when data from RS is available) is used to illustrate

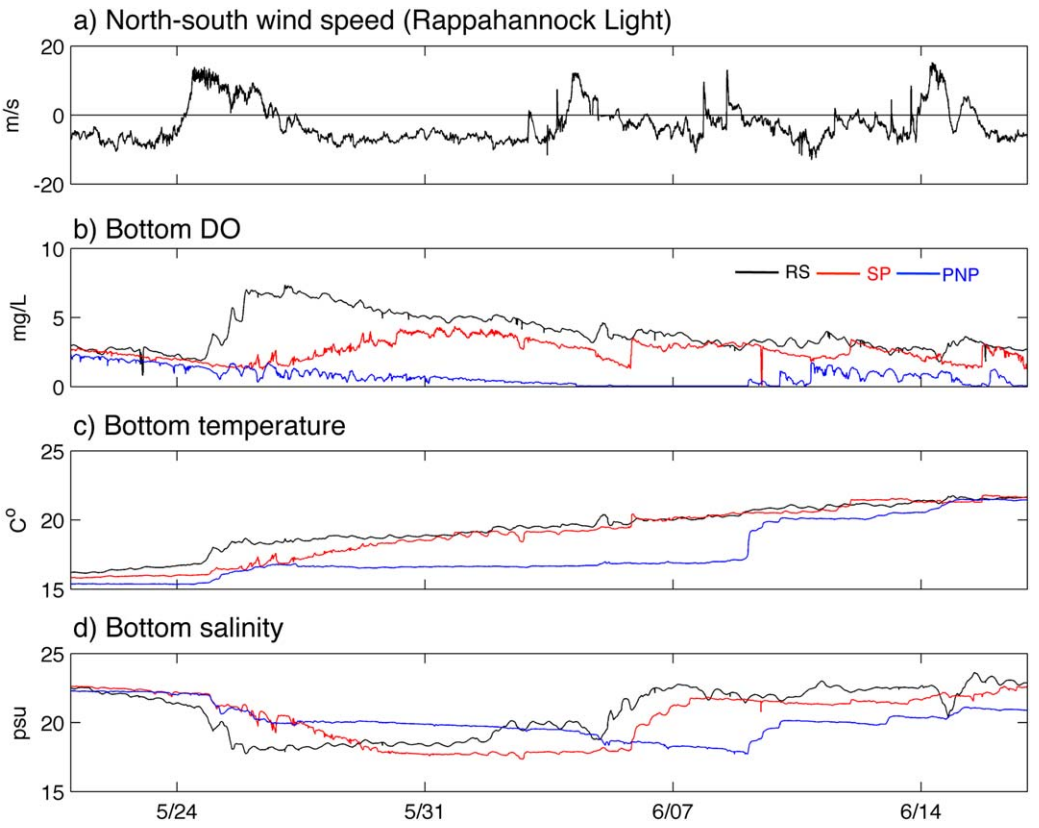

Figure 13. Time series of (a) north-south wind velocity at Rappahannock Light (NDBC station RPLV2); (b) bottom dissolved oxygen; (c) bottom temperature; and (d) bottom salinity at RS (black line), SP (red line), and PNP (blue line) during May–June 2013. The increase in dissolved oxygen and temperature and the decrease in salinity observed at RS occurs during the strong wind event from the north, consistent with vertical mixing. The signal is observed much later at SP and PNP, due to northward advection.

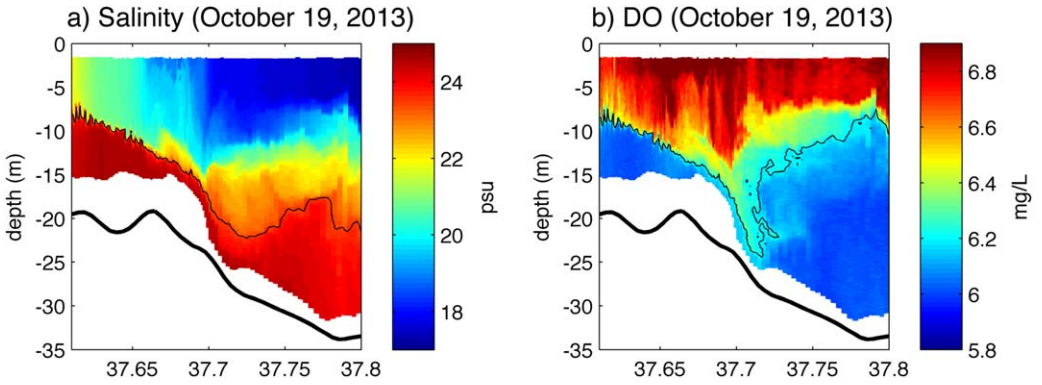

Figure 14. Contours of (a) salinity and (b) dissolved oxygen collected during an along-Bay Scanfish survey on 19 October 2013 in the region where the deep channel shoals rapidly onto Rappahannock Shoal. Black line in Figure 14a is the 23.5 psu contour and the black line in Figure 14b is the 6.2 mg/L contour, which are shown to highlight the inferred downwelling and mixing that occurs because of surface convergence in this region.

one such event. The event begins early on 24 May, prior to which, winds were blowing from the south. During the event, sustained winds from the north exceed 10 m/s and the duration of down-Bay winds is roughly 2.25 days (Figure 13a). The rapid increase in DO at RS corresponds to the increase in winds from the north (Figure 13b). The increase in DO at RS is accompanied by an increase in water temperature and a decrease in salinity (Figures 13c and 13d), consistent with vertical mixing. The increase in bottom DO at SP is not observed until several days after the increase at RS, and occurs after the winds have subsided. The increase in bottom DO at SP also coincides with a decrease in salinity and increase in temperature, consistent with the northward advection of warmer, fresher, and more oxygenated water that was created by mixing over Rappahannock Shoal during the wind event.

The oxygenated water that arrives at RS and SP has a salinity of $\sim$18 psu and a temperature greater than 18°C (Figures 13c and 13d). At PNP, the bottom DO continues to decrease after the wind event eventually approaching anoxic conditions, and the bottom temperature remains below 17°C. DO does not increase above $\sim$0 mg/L until 9 June. The increase in DO at PNP is accompanied by a rapid increase in temperature ($>$18°C) and the arrival of water with a salinity of $\sim$18 psu, consistent with the water mass that was observed at RS and SP, during and immediately following the wind event. The data suggest that the increase in oxygen observed at PNP on 9 June resulted from the northward advection of water that was mixed over Rappahannock Shoal during the wind event on 24 May. The increase in DO at PNP is much smaller than that observed at RS and SP, presumably because biological utilization reduced the DO concentration during the $\sim$17 day transit. The simple advective balance shown in Figure 12 does not account for oxygen utilization and advection cannot explain the decrease in DO that is observed at PNP during late May and into June, partially explaining the poor correlation seen in Figure 12 for the first deployment.

The axial Scanfish survey conducted on 18–19 October 2013 provides qualitative evidence that localized vertical mixing occurs south of SP where the deep channel shoals rapidly onto Rappahannock Shoal (Figure 14). There is a relatively strong surface salinity front at 37.67°N and the fresh surface layer thickens considerably as the depth shoals in the down-Bay direction. The strong downwelling at this location is evident in the DO field, with the 6.2 mg/L contour plunging almost all the way to the bottom. On the top of the shoal, there are well-defined surface and bottom layers separated by a strong interface in both salinity and DO. Over the sloping region north of the shoal, the interface is much thicker and less defined, consistent with vertical mixing.

The Scanfish data demonstrate that the surface convergence and associated downwelling and mixing can bring fresh and more oxygenated waters to depth. The period when the vessel was transiting Rappahannock Shoal occurred during the transition from an ebb to a flood tide. As the vessel reach the top of the shoal, the surface currents measured at SP were essentially zero and the near bottom flow was flooding weakly. The Scanfish data suggest that fresher more oxygenated water is being entrained into the flooding near bed currents (Figure 14b). Thus, it appears that the relatively rapid change in depth associated with Rappahannock Shoal results in surface convergence and downwelling, which result in localized mixing that

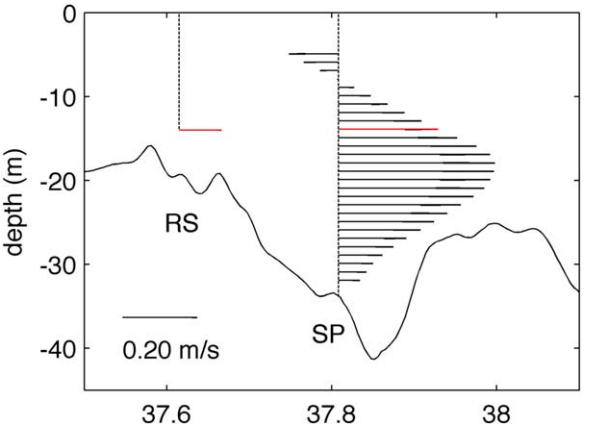

Figure 15. Vertical profile of subtidal along-channel velocity at SP and vector of bottom current at RS, averaged over the down-Bay wind event (24–27 May 2013). Velocity vectors are shown relative to the along-channel bathymetry. Surface downwelling is inferred to satisfy the strong horizontal divergence in the residual flow at $z = -14$ m.

brings fresher and more oxygenated water to the bottom. This fresher more oxygenated water can be advected up-Bay, resulting in the up-Bay propagation of higher DO and lower salinity water.

The Scanfish survey on 18–19 October was conducted under relatively weak wind forcing. Subtidal surface currents in Chesapeake Bay respond strongly to surface wind forcing (e.g., Figure 7) and under strong down-Bay winds the surface convergence and downwelling on the northern flank of Rappahannock Shoal is most likely intensified. Following the strong north wind event in late May, the salinity at SP decreases to values that are lower than observed at RS and PNP, consistent with downwelling occurring north of RS. During the north wind event, the near-bed subtidal flow at RS is directed up-Bay, as is the subtidal flow at SP at the same depth (~ -14 m) (Figures 15 and 16b). The flow at $z \sim -14$ m at SP is much stronger than at RS, implying a strong horizontal divergence at this depth. At the surface, the down-Bay wind results in an enhanced down-Bay subtidal flow at SP (Figure 16c). Although we do not have direct measurements of surface currents at RS, we infer strong convergence in the down-estuary surface flow which would result in downwelling to satisfy the observed horizontal divergence in the flow at $z \sim -14$ m. The inference of strong convergence in the down-Bay directed surface flow is supported by the

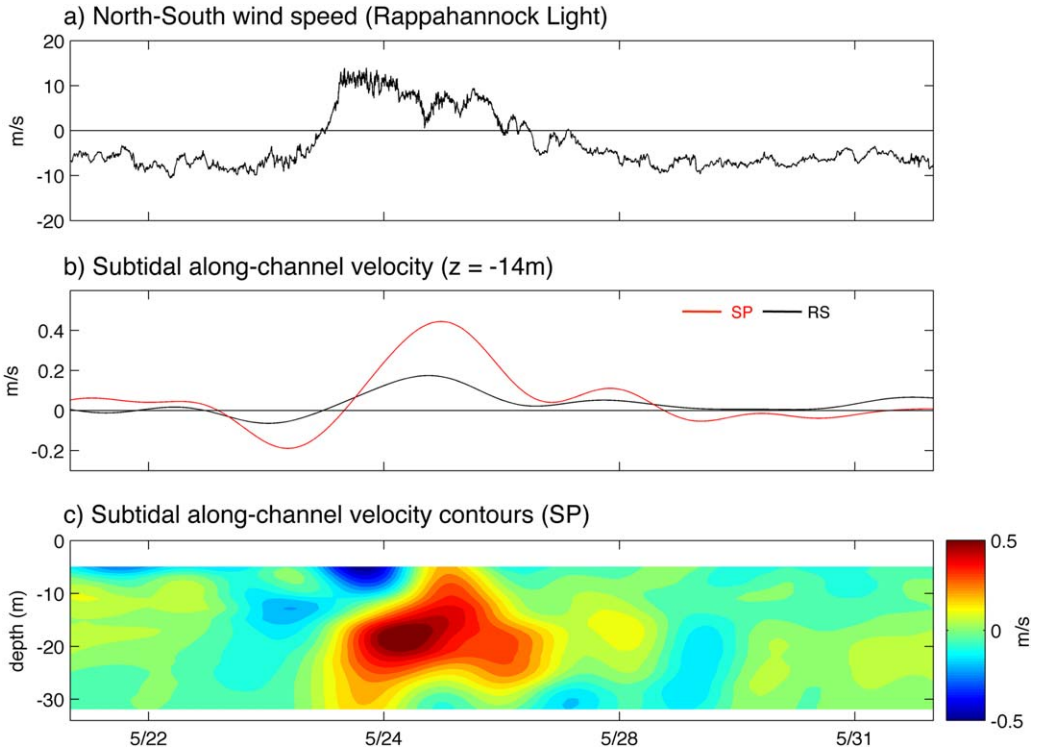

Figure 16. (a) North-south wind speed at Rappahannock Light during strong down-Bay wind event in late May 2013; (b) corresponding subtidal along-channel velocity measured at RS (black line) and SP (red line), both 14 m below the mean water surface; and (c) contours of subtidal along-channel velocity measured at SP during the down-Bay event. Positive values are directed up-Bay. As the wind event progresses, the surface flow at SP becomes arrested (and reverses), even though winds are still from the north.

subtidal velocities at SP, which show that the outflow in the surface layer becomes arrested and reverses, even though the winds are still strongly from the north (Figure 16c).

It is unlikely that the entrainment process suggested by Figure 14 is responsible for all of the oxygenated water that propagates up the Bay. More likely, broad mixing over Rappahannock Shoal is the source of this oxygenated water. To illustrate the importance of this region, the volume of water over Rappahannock Shoal is compared to volume of subpycnocline water to the north. Rappahannock Shoal is defined crudely from the bathymetry as the region between 37.2°N and 37.7°N that has a depth less than 15 m. Similarly, the subpycnocline waters of the Bay are defined crudely as of the integrated volume deeper than $z = -15$ m that is north of 37.7°N. In both calculations, any volume associated with the tributaries is excluded from the calculation. The volume of water over Rappahannock Shoal ($\sim$13.6 km^3) is over 5 times greater than the volume of subpycnocline water to north ($\sim$2.3 km^3). This suggests that even if only a relatively small fraction of the water mixed over the Rappahannock Shoal is transported up Bay, it is more than sufficient to fill a significant fraction of the subpycnocline volume to the north with oxygenated water.

4. Discussion and Conclusions

The observations of the lateral response to along-Bay wind forcing are generally consistent with previous numerical model simulations in Chesapeake Bay [*Li and Li*, 2012]. In particular these observations demonstrate that the lateral response is consistent with Ekman dynamics with a clear asymmetry between the response to along-Bay winds and across-Bay winds. *Scully* [2010a] documented that there was a strong negative correlation between the percent duration of winds from the west and observations of hypoxic volume for the period 1950–2007. It was suggested that the lateral response to along-Bay wind forcing played a fundamental role in supplying oxygen to subpycnocline waters and that more frequent winds from the west favored increased hypoxic volume. The observations presented above generally support this conclusion.

The observed lateral response is consistent with wind-driven Ekman dynamics and the first-order thermal wind balance in the lateral momentum balance suggests that interior pycnocline waters remain essentially inviscid during moderate wind forcing. Yet the lateral response to along-Bay winds can raise or lower the pycnocline into the surface or bottom boundary layer where vertical mixing can occur. Even though the lateral response is consistent with the thermal wind balance, it provides a mechanism to enhance mixing at the periphery of hypoxic regions limiting their growth. Even under extremely strong wind forcing (e.g., Hurricane Irene) advection by the rotational response plays an important role in supplying oxygenated water to the bottom. The rotational response also drives asymmetries in where the surface oxygen flux occurs, with enhanced influx on the western shore during up-Bay winds and enhanced influx on the eastern shore during down-Bay winds. This mechanism has been suggested by numerical simulations [*Scully*, 2010b], but the field data presented above provide direct observational support.

The importance of the rotational response to along-Bay winds is not surprising. The Kelvin number (K_e) [*Garvine*, 1995] in Chesapeake Bay is generally greater than 1, suggesting that the system is wide relative to the internal Rossby radius [*Li and Li*, 2011, 2012]. It is perhaps more instructive to think about the rotational response of an estuarine system in terms of the ratio of time scales than the ratio of length scales. The Ekman number (E_k) can be thought of as the ratio of the frictional time scale to the rotational time scale [*Kasai et al*., 2000; *Winant*, 2004; *Valle-Levinson*, 2008]. Numerical simulations show that values of the eddy viscosity in the pycnocline of Chesapeake Bay are seldom, if ever, above the model's background viscosity [*Li et al*., 2005; *Scully*, 2010b], indicating that $E_k \ll 1$. This bulk scaling highlights that in the absence of significant interfacial friction between the surface and bottom layers, there will be a rotational response to wind forcing.

The rotational response to wind forcing is expected to be important to oxygen dynamics in other wide ($K_e > 1$) and deep ($E_k < 1$) stratified systems. Mobile Bay is wide with $K_e > 1$ [*Noble et al*., 1996]. There is a deep shipping channel ($\sim$20 m) flanked by broad shallow shoals and the system experiences significant density stratification and hypoxia [*Turner et al*., 1987]. The well-known "jubilee" events are thought to be caused by wind forcing [*May*, 1973] and the earth's rotation likely contributes to the advection of low oxygen water into the shallow regions of the Bay. Long Island Sound is a relatively deep and wide system that

exhibits a rotational response to wind forcing [*Whitney and Codiga*, 2011], suggesting that similar lateral processes may also be important to oxygen dynamics there as well.

The data presented in this paper also highlight the importance that wind forcing plays in controlling oxygen dynamics in the along-channel direction. Estimates of the Wedderburn number for Chesapeake Bay are typically greater than 1, even for relatively weak wind events [*Li and Li*, 2011], suggesting that the along-channel wind stress contributes significantly to the subtidal circulation. Down-Bay winds result in strong surface convergence and downwelling near Rappahannock Shoal with localized mixing in this region where the bottom bathymetry shoals rapidly. The bottom sensors demonstrate that increases in DO concentration are often associated with decreases in salinity, increases in temperature, and up-Bay residual currents. The observed increases in DO appear to propagate up the Bay and the time rate of change in bottom DO is largely consistent with along-channel advection. Modeling studies of oxygen dynamics in Chesapeake Bay suggest that along-channel advection of oxygen plays an important role in controlling the extent and severity of summertime hypoxia. *Li et al*. [2015] conclude that both down-estuary winds and increased river discharge enhance the near bed residual flow and hence the up-Bay advective flux of oxygen. *Scully* [2013] found similar results and suggested that changes in the longitudinal advective fluxes associated with changes in wind direction contributed significantly to the seasonal cycle of hypoxia.

These previous modeling studies did not identify the importance of strong surface convergence and the associated downwelling and mixing near Rappahannock Shoal, and the results presented here show subtle but important differences from previous modeling studies. The influx of oxygen is not carried by salty oxygen-rich oceanic waters, but rather by fresher oxygen-rich water that is created by localized mixing. Mixing in this region appears to be enhanced by the surface convergence and downwelling in the vicinity of Rappahannock Shoal during winds from north, which are much more common during the fall and winter than during the summer months. It is possible that these advective processes are the dominant source of DO to the subpycnocline waters of Chesapeake Bay and the lack of strong wind forcing from the north during the summer is the primary physical reason that hypoxia develops.

The importance of Rappahannock Shoal is analogous to the intensified mixing at a sill near the mouth of a fjord. The mixing in this region is important to the dynamics of the interior basin and can control the renewal of deep water [*Geyer and Cannon*, 1982]. In Puget Sound, there is significant flow blockage, recirculation, and intense mixing at several sills throughout the system [*Ebbesmeyer and Barnes*, 1980]. These regions are important to the supply of DO to the interior basins and play an important role in modulating hypoxia. Western Long Island Sound is separated from the deeper waters near its mouth by Mattituck Sill, and mixing in this region may supply the bottom waters to the west with oxygen via horizontal advection. *O'Donnell et al*. [2008] show that ventilation events in Long Island Sound are strongly dependent upon wind direction and are the result of both mixing and horizontal advection.

In deep estuarine systems with persistent stratification, it is unlikely that direct vertical mixing through the pycnocline is the dominant source of oxygen to bottom waters. Chesapeake Bay maintains vertical stratification nearly year round. The passage of Hurricane Irene reduced, but did not erase, the vertical density stratification. The gradient Richardson number in the pycnocline over the deep channel is almost always greater than 1 [*Scully*, 2010b], suggesting that there is essentially no direct turbulent mixing through the pycnocline. The results presented in this paper demonstrate that mixing in these deep estuarine systems cannot be thought of as a simple 1-D process in the vertical, but rather a complex 3-D processes that is heterogeneous in both time and space. Oxygen is not supplied to subpycnocline waters directly by vertical mixing, but rather by advective processes.

Acknowledgments
Funding for this research was provided by the National Science Foundation grant OCE-1338518. The data presented in this manuscript are available upon request through the corresponding author (mscully@whoi.edu).

References

Butt, A. J., and B. L. Brown (2000), The cost of nutrient reduction: A case study of Chesapeake Bay, *Coastal Manage.*, *28*, 175–185.
Ebbesmeyer, C. C., and C. A. Barnes (1980), Control of a fjord basin's dynamics by tidal mixing in embracing sill zones, *Estuarine Coastal Mar. Sci.*, *11*(3), 311–330.
Garvine, R. W. (1995), A dynamical system for classifying buoyant coastal discharges, *Cont. Shelf Res.*, *15*(13), 1585–1596.
Geyer, W. R., and G. A. Cannon (1982), Sill processes related to deep water renewal in a fjord, *J. Geophys. Res.*, *87*(C10), 7985–7996.
Hagy, J. D., W. R. Boyton, C. W. Keefe, and K. V. Wood (2004), Hypoxia in Chesapeake Bay, 1950-2001: Long-term changes in relation to nutrient loading and river flow, *Estuaries*, *27*, 634–658.
Kasai, A., A. E. Hill, T. Fujiwara, and J. H. Simpson (2000), Effect of the Earth's rotation on the circulation in regions of freshwater influence, *J. Geophys. Res.*, *105*(C7), 16,961–16,969.

Kemp, W. M., J. M. Testa, D. J. Conley, D. Gilbert, and J. D. Hagy (2009), Temporal responses of coastal hypoxia to nutrient loading and physical controls, *Biogeosciences*, *6*(12), 2985–3008.
Li, M., L. Zhong, and W. C. Boicourt (2005), Simulations of Chesapeake Bay estuary: Sensitivity to turbulence mixing parameterizations and comparison with observations, *J. Geophys. Res.*, *110*, C12004, doi:10.1029/2004JC002585.
Li, Y., and M. Li (2011), Effects of winds on stratification and circulation in a partially mixed estuary, *J. Geophys. Res.*, *116*, C12012, doi: 10.1029/2010JC006893.
Li, Y., and M. Li (2012), Wind-driven lateral circulation in a stratified estuary and its effects on the along-channel flow, *J. Geophys. Res.*, *117*, C09005, doi:10.1029/2011JC007829.
Li, Y., M. Li, and W. M. Kemp (2015), A budget analysis of bottom-water dissolved oxygen in Chesapeake Bay, *Estuaries Coasts*, *38*(6), 2132–2148.
Malone, T. C., W. M. Kemp, H. W. Ducklow, W. R. Boynton, J. H. Tuttle, and R. B. Jonas (1986), Lateral variation in the production and fate of phytoplankton in a partially stratified estuary, *Mar. Ecol. Prog. Ser.*, *32*, 149–160.
May, E. B. (1973), Extensive oxygen depletion in Mobile Bay, Alabama, *Limnol. Oceanogr.*, *18*(3), 353–366.
Murphy, R. R., W. M. Kemp, and W. P. Ball (2011), Long-term trends in Chesapeake Bay seasonal hypoxia, stratification and nutrient loading, *Estuaries Coasts*, *34*, 1293–1309.
Noble, M. A., W. W. Schroeder, W. J. Wiseman, H. F. Ryan, and G. Gelfenbaum (1996), Subtidal circulation patterns in a shallow, highly stratified estuary: Mobile Bay, Alabama, *J. Geophys. Res.*, *101*(C11), 25,689–25,703.
O'Donnell, J., H. G. Dam, W. F. Bohlen, W. Fitzgerald, P. S. Gay, A. E. Houk, D. C. Cohen, and M. M. Howard-Strobel, (2008), Intermittent ventilation in the hypoxic zone of western Long Island Sound during the summer of 2004, *J. Geophys. Res. Oceans*, *113*, C9, doi:10.1029/2007JC004716.
Officer, C. B., R. B. Biggs, J. L. Taft, L. E. Cronin, M. A. Tyler, and W. R. Boynton (1984), Chesapeake Bay Anoxia: Origin, development, and significance, *Science*, *223*, 22–27.
Sanford, L. P., K. G. Sellner, and D. L. Breitburg (1990), Covariability of dissolved oxygen with physical processes in the summertime Chesapeake Bay, *J. Mar. Res.*, *48*, 567–590.
Scully, M. E. (2010a), The importance of climate variability to wind-driven modulation of hypoxia in Chesapeake Bay, *J. Phys. Oceanogr.*, *40*, 1435–1440.
Scully, M. E. (2010b), Wind modulation *of dissolved oxygen in Chesapeake Bay, Estuaries Coasts, 33, 1164–1175*.
Scully, M. E. (2013), Physical controls on hypoxia in Chesapeake Bay: A numerical modeling study, *J. Geophys. Res. Oceans*, *118*(3), 1239–1256.
Seliger, H. H., J. A. Boggs, and W. H. Biggley (1985), Catastrophic anoxia in the Chesapeake Bay in 1984, *Science*, *228*, 70–73.
Taft, J. L., W. R. Taylor, E. O. Hartwig, and R. Loftus (1980), Seasonal oxygen depletion in Chesapeake Bay, *Estuaries*, *3*, 242–247.
Turner, R. E., W. W. Schroeder, and W. J. Wiseman (1987), The role of stratification in the deoxygenation of Mobile Bay and adjacent shelf bottom waters, *Estuaries*, *10*(1), 13–19.
Valle-Levinson, A. (2008), Density-driven exchange flow in terms of the Kelvin and Ekman numbers, *J. Geophys. Res. Oceans*, *113*, C4, doi: 10.1029/2007JC004144.
Wanninkhof, R. (1992), Relationship between wind speed and gas exchange over the ocean, *J. Geophys. Res. Oceans*, *97*(C5), 7373–7382.
Whitney, M. M., and D. L. Codiga (2011), Response of a large stratified estuary to wind events: Observations, simulations, and theory for Long Island Sound, *J. Phys. Oceanogr.*, *41*(7), 1308–1327.
Winant, C. D. (2004), Three dimensional wind-driven flow in an elongated rotating basin, *J. Phys. Oceanogr.*, *34*(2), 462–476.